University of Reading

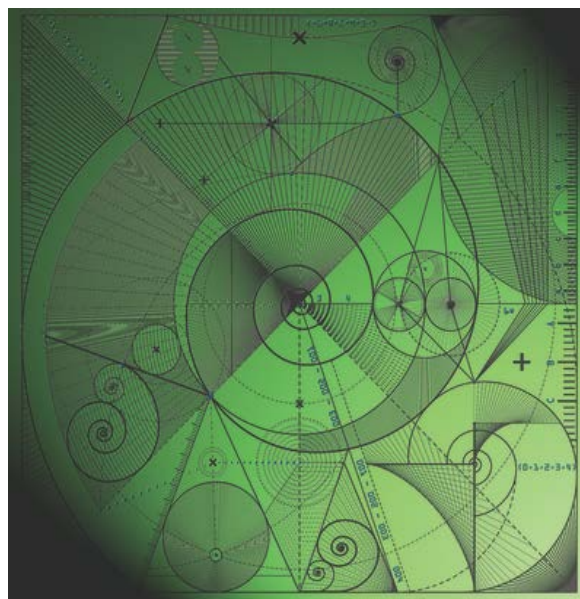# Department of Mathematics and Statistics

7 August 2015

A moving point approach to model shallow ice sheets: a study case with radially-symmetrical ice sheets

by

B. Bonan, **M.J. Baines**, **N.K. Nichols** and D. Partridge

A moving point approach to model shallow ice sheets: a study case with radially-symmetrical ice sheets[*]

B. Bonan[†1], M.J. Baines[1], N.K. Nichols[1], and D. Partridge[1]

[1]School of Mathematical and Physical Sciences, University of Reading, Reading, Berkshire, United Kingdom

August 7, 2015

Abstract

Predicting the evolution of ice sheets requires numerical models able to accurately track the migration of ice sheet continental margins or grounding lines. We introduce a physically-based moving point approach for the flow of ice sheets based on the conservation of local masses. This allows the ice sheet margins to be tracked explicitly and the waiting time behaviours to be modelled efficiently. A finite difference moving point scheme is derived and applied in a simplified context (continental radially-symmetrical shallow ice approximation). The scheme, which is inexpensive, is validated by comparing the results with moving-margin exact solutions and steady states. In both cases the scheme is able to track the position of the ice sheet margin with high precision.

1 Introduction

Ice loss in Greenland and Antarctica accounts for a large fraction of today's sea-level rise (Church et al., 2013). This ice loss modifies the ice flow but also translates into the retreat of continental margins (in Greenland) and grounding lines (mainly in Antarctica). Predicting the evolution of both aspects is essential in order to accurately estimate their future contribution to sea-level change. However, simulating the migration of an ice sheet margin or a grounding line remains a complex task (see e.g. Vieli and Payne, 2005; Pattyn et al., 2013). This paper introduces a moving point method for the numerical simulation of ice sheets, especially the migration of their boundaries. In this paper we focus on the migration of continental ice sheet margins.

At the scale of an ice sheet or a glacier, ice is modelled as a flow which follows the Stokes equations of fluid flows (Stokes, 1845), even though the flow is non-Newtonian and its rheology is highly nonlinear. Solving this problem at that scale is costly. A 3-D finite element model called Elmer/Ice has been developed for this purpose numerically (see Gagliardini et al., 2013 for a detailed description of Elmer/Ice). Other models take advantage of the very small aspect ratio of ice sheets and use a thin layer approximation differing only in the order of the approximation. The oldest and numerically least expensive model used for ice flow is the Shallow Ice

---

[†]email: `b.c.bonan@reading.ac.uk`

Approximation or SIA (Hutter, 1983). It gives an analytical formulation for horizontal velocities of ice in the sheet and for their vertically averaged counterpart. Although simple and fast, the SIA captures well the nonlinearity of the system and is an excellent resource for testing numerical approaches, since moving-margin exact solutions exist in the literature (Halfar, 1981, 1983; Bueler et al., 2005).

Significant efforts have been invested in ice sheet modelling. These have led ice sheet modellers to compare results obtained by various models for the same idealistic test problems (see the EISMINT intercomparison project (Huybrechts et al., 1996; Payne et al., 2000) for ice sheet models using SIA). Most numerical ice sheet simulations use a fixed grid to calculate the solution of the ice flow equations. In fixed grid models the ice sheet margins are not precisely located as they generally fall between grid points. So in order to obtain a good approximation a high grid resolution is required around the positions of the ice sheet margin during its evolution, which makes fixed grid models costly for accurately computing the evolution of the ice margin.

One approach to gain high resolution is to apply adaptative grid techniques, which allow improved resolution to be achieved in key areas. For example, Cornford et al. (2013) apply adaptative mesh refinement (AMR) in the case of marine ice sheets and grounding line migration. However, even with AMR, the ice sheet margin still falls between grid points, although by adapting the grid to increase the resolution near the margin, the accuracy is kept high. Adapting the grid is, nevertheless, an expensive procedure, as areas where refinement is needed have to be regularly re-identified.

Another possibility is to transform the moving domain. The number of grid points is kept constant in time but the accuracy is kept high by the explicit tracking of the position of the ice sheet margin. This is done by transforming the ice domain to a stretched coordinate system via a geometric transformation. This approach has been succesfully applied by Hindmarsh (1993) and Hindmarsh and Le Meur (2001) to a marine ice sheet along a flowline. However, it is not easily translated into two dimensions and no pure transformed grid ice sheet model has been published.

We consider here intrinsically moving grid methods. As in the case of transformed grids, these methods allow explicit tracking of the ice sheet margin. There exists a number of techniques for generating the nodal movement in moving grid methods. They can be classified into two subcategories, location-based methods and velocity-based methods (Cao et al., 2003). In location-based methods the positions of the nodes are redefined directly at each time step by a mapping from a reference grid (Budd et al., 2009). This is generally done by choosing a monitor function. In velocity-based methods, on the other hand, the movement of the nodes is defined in terms of a time-dependent velocity, which allows the nodes to be influenced by their previous position (Baines et al., 2005, 2011). Currently, this approach has not been applied to the dynamics of ice sheets and we address the issue in this paper.

In this paper, we apply a particular velocity-based moving point approach based on conservation of local mass fractions to continental ice sheets. We derive a finite difference moving point scheme in a simplified context and validate the approach with known exact solutions in the case of radially-symmetrical ice sheets. We show in particular that the scheme is able to track the position of the ice sheet margin accurately. The paper is organised as follows: in Sect. 2 we recall the SIA and detail the simplified context of our study, in Sect. 3 we describe our velocity-based moving point approach, and in Sect. 4 we validate our approach by comparison with exact solutions before concluding in Sect. 5.

2 Ice sheet modelling

2.1 Ice sheet geometry and Shallow Ice Approximation

We consider a single solid phase ice sheet whose thickness at position (x, y) and time t is denoted by $h(t, x, y)$. We assume that the ice sheet lies on a fixed bedrock and denote by $b(x, y)$ the bed elevation. The surface elevation, $s(t, x, y)$, is then obtained as

$$s = b + h \tag{1}$$

The evolution of ice sheet thickness is governed by the balance between ice gained or lost on the surface, snow precipitation and surface melting, and ice flow draining ice accumulated in the interior towards the edges of the ice sheet. This is summarised in the mass balance equation

$$\frac{\partial h}{\partial t} = m - \boldsymbol{\nabla} \cdot (h\mathbf{U}) \quad \text{in} \ \ \Omega(t) \tag{2}$$

where $m(t, x, y)$ is the surface mass balance (positive for accumulation, negative for ablation), $\mathbf{U}(t, x, y)$ is the vector containing the vertically averaged horizontal components of the velocity of the ice, and $\Omega(t)$ is the area where the ice sheet is located.

Formally derived by Hutter (1983), the Shallow Ice Approximation (SIA) is one of the most common approximations for large-scale ice sheet dynamics. Combined with Glen's flow law (Glen, 1955), the SIA provides (in the isothermal case) an analytical formulation for $\mathbf{U}$ as follows:

$$\mathbf{U} = -\frac{2}{n+1} A \left(\rho_i g\right)^n \, h^{n+1} \left|\boldsymbol{\nabla} s\right|^{n-1} \boldsymbol{\nabla} s \tag{3}$$

Parameters involved in this formulation are summarised in Table 1. Regarding the exponent $n > 1$, its fixed value is classically set to 3 (see Cuffey and Paterson, 2010, for more details).

2.2 Radially-symmetrical ice sheets

This paper describes and assesses the use of a moving point approach to model ice sheet evolution based on conservation of mass fraction. As a first step, we confine the study to limited area ice sheets with radial symmetry, in other words, $\Omega(t) = [0, r_l(t)] \times [0, 2\pi]$. The ice sheet is centred on $(0, 0)$ and $r_l(t)$ denotes the position of the ice sheet margin (edge of the ice sheet) at time t (see Fig. 1). The radial symmetry implies that the geometry of the sheet depends only on r, so $h(t, x, y) = h(t, r)$, $s(t, x, y) = s(t, r)$ and $b(x, y) = b(r)$. The vector $\mathbf{U}$ can then be written in the radial coordinate system as

$$\mathbf{U} = U\,\hat{\mathbf{r}}, \quad U = -\frac{2}{n+2} A \, (\rho_i g)^n h^{n+1} \left|\frac{\partial s}{\partial r}\right|^{n-1} \frac{\partial s}{\partial r} \tag{4}$$

Table 1: Parameters involved in the computation of the vertically averaged horizontal components of the velocity of the ice.

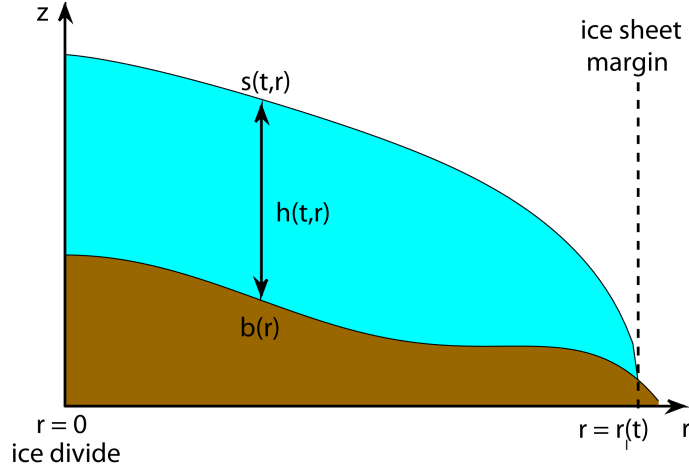| Parameter	Meaning	Value
n	exponent in Glen flow law	3
A	Glen flow law coefficient	10^{-16} Pa^{-3}.a^{-1}
ρ_i	density of ice	910 kg.m^{-3}
g	gravitational acceleration	9.81 m.s^{-2}

Figure 1: Section of a grounded radially-symmetrical ice sheet.

where $\hat{\mathbf{r}}$ is the unit radial vector, and the mass balance Eq. (2) simplifies to

$$\frac{\partial h}{\partial t} = m - \frac{1}{r}\frac{\partial\left(r\,h\,U\right)}{\partial r} \tag{5}$$

A symmetry condition is added at the ice divide ($r = 0$):

$$U = 0 \quad \text{and} \quad \frac{\partial s}{\partial r} = 0, \tag{6}$$

and the ice sheet margin $r_l(t)$ is characterised by the Dirichlet boundary condition:

$$h(t, r_l(t)) = 0 \tag{7}$$

We also assume that the flux of ice through the ice sheet margin is zero (no calving).

The aim of this paper is to propose a moving point numerical method able to accurately simulate the evolution of the ice sheet margin. Under some hypotheses regarding the regularity of the ice thickness near the margin (see Calvo et al., 2002), we can differentiate Eq. (7) with respect to time. If $\partial h/\partial r$ does not tend to zero near the margin, we obtain the following equation

$$\frac{\mathrm{d}r_l}{\mathrm{d}t} = U(t, r_l(t)) - m(t, r_l(t))\left(\frac{\partial h}{\partial r}\right)^{-1} \tag{8}$$

This equation (Eq. 8) will be used in the moving point approach described in the next section.

3   A moving point approach

In the following paragraphs we describe the moving point method that we use to simulate the dynamics of ice sheets in the context of Sect. 2.2. This method is essentially a velocity-based (or Lagrangian) method relying on the construction of velocities for grid points at each instant of time. This allows the grid to move with the flow of ice. Moving points cover the domain only where the ice sheet exists, so that no grid point is wasted. Adjacent points move to preserve local mass fractions and the movement is thus based on the physics (Blake, 2001; Baines et al.,

2005, 2011; Scherer and Baines, 2012; Lee et al., 2015). This conservation method has been applied in various contexts and is perfectly suitable for multi-dimensional problems (different examples are summarised in Baines et al. (2011) and references therein; see also Partridge (2013) for the special case of ice sheet dynamics). The key points of the method are given in the next paragraphs and the numerical validation of the method is carried out in Sect. 4.

3.1 Conservation of mass fraction

Moving point velocities are derived from the conservation of mass fractions (CMF). To apply this principle we first define the total mass of the ice sheet $\theta(t)$ as

$$\theta(t) = 2\pi \int_0^{r_l(t)} r\, h(t, r)\, \mathrm{d}r \tag{9}$$

In fact $\theta(t)$ is the total volume of the ice sheet but, since the density of ice is assumed constant everywhere, $\theta(t)$ is proportional to the total mass of the ice sheet and the constant of proportionality cancels out.

Since the flux of ice through the ice sheet margin is assumed to be zero, any change in the total mass over the whole ice sheet is due solely to the surface mass balance $m(t, r)$, and hence the rate of change of the total mass, $\dot{\theta}$, is given by

$$\dot{\theta}(t) = 2\pi \int_0^{r_l(t)} r\, m(t, r)\, \mathrm{d}r \tag{10}$$

We now introduce the principle of the conservation of mass fractions. Let $\hat{r}(t)$ be a moving point and define $\mu(\hat{r})$ to be the *relative* mass in the moving subinterval $(0, \hat{r}(t))$ as

$$\mu(\hat{r}) = \frac{2\pi}{\theta(t)} \int_0^{\hat{r}(t)} r\, h(t, r)\, \mathrm{d}r \tag{11}$$

The rate of change of $\hat{r}(t)$ is determined by keeping $\mu(\hat{r})$ independent of time for all moving subdomains of $[0, r_l(t)]$. Note that $\mu(\hat{r}) \in [0, 1]$ is a cumulative function with $\mu(0) = 0$ and $\mu(r_l) = 1$.

3.2 Trajectories of moving points

We obtain the velocity of a moving point by differentiating Eq. (11) with respect to time, giving

$$\frac{\mathrm{d}}{\mathrm{d}t}\left(2\pi \int_0^{\hat{r}(t)} r\, h(t, r)\, \mathrm{d}r\right) = \mu(\hat{r})\, \dot{\theta}(t) \tag{12}$$

Carrying out the time differentiation using Leibniz's integral rule and substituting for $\partial h/\partial t$ from the mass balance Eq. (5) gives

$$\frac{\mathrm{d}}{\mathrm{d}t}\left(\int_0^{\hat{r}(t)} r\, h(t, r)\, \mathrm{d}r\right) = \int_0^{\hat{r}(t)} r\, m(t, r)\, \mathrm{d}r + \hat{r}(t)\, h(t, \hat{r}(t))\left(\frac{d\hat{r}}{dt} - U(t, \hat{r}(t))\right) \tag{13}$$

with boundary conditions (Eq. 6) at $r = 0$. From Eqs. (12), (13) and (10), we can determine the velocity of every interior point as

$$\frac{\mathrm{d}\hat{r}}{\mathrm{d}t} = U(t, \hat{r}(t)) + \frac{1}{\hat{r}(t) h(t, \hat{r}(t))}\left(\mu(\hat{r}) \int_0^{r_l(t)} r\, m(t, r)\, \mathrm{d}r - \int_0^{\hat{r}(t)} r\, m(t, r)\, \mathrm{d}r\right) \tag{14}$$

5

The point at $r = 0$ is located at the ice divide, which does not move during the simulation. The point at $r_l(t)$ is dedicated to the ice sheet margin, which moves with the velocity obtained in Eq. (8). We verify in Appendix A that the interior velocity calculated by Eq. (14) coincides with the boundary velocities calculated directly from the boundary conditions (see Eq. 8).

3.3 Determination of the ice thickness profile

Once the velocities $\mathrm{d}\hat{r}/\mathrm{d}t$ of the moving points $\hat{r}(t)$ have been found from Eq. (14), the points are moved in a Lagrangian manner. In addition, the total mass $\theta(t)$ is updated from Eq. (10). The ice thickness profile is then deduced from Eq. (11) as follows. Differentiating Eq. (11) with respect to $\hat{r}^2$, we obtain

$$h(t, \hat{r}(t)) = \frac{\theta(t)}{\pi} \frac{\mathrm{d}\mu(\hat{r})}{\mathrm{d}(\hat{r}^2)} \tag{15}$$

which allows the ice thickness profile at time t to be constructed since $\mathrm{d}\mu(\hat{r})/\mathrm{d}(\hat{r}^2)$ is constant in time and therefore known from the initial data. Note that the positivity of the ice thickness is preserved since μ is by definition a strictly increasing function (see Eq. 11).

3.4 Asymptotic behaviour at the ice sheet margin

As pointed out by Fowler (1992) and Calvo et al. (2002), with SIA singularities can appear at the margin of grounded ice sheets. The singularity arises because of the vanishing of h at the margin and the steepening of the slope $\partial h/\partial r$. Nevertheless the ice velocity U defined by Eq. (4) can remain finite even if the slope is infinite. We give more details on this subject in this subsection. We also detail the influence of the singularity on the movement of the ice sheet margin.

At a fixed time and for points r sufficiently close to r_l, we can write the ice thickness profile $h(r)$ as the first term in a Frobenius expansion

$$h(r) = (r_l - r)^{\gamma} g_l \tag{16}$$

to leading order, where $g_l = O(1)$. If $\gamma = 1$, then $h(r)$ is locally linear with slope g_l, but if $\gamma < 1$ the slope $\partial h/\partial r$ is unbounded. Hence in the asymptotic region near the margin, in the case where the bedrock topography $b(r)$ is constant, from Eq. (4)

$$U = \frac{2}{n+2} A \, (\rho_{\mathrm{i}} g)^n \gamma^n (r_l - r)^{(2n+1)\gamma - n} g_l^{2n+1} \tag{17}$$

which vanishes as r tends to r_l if $\gamma > n/(2n+1)$ and remains finite if $\gamma = n/(2n+1)$.

Supppose that in the evolution of the solution over time, $\gamma(t) > n/(2n+1)$ initially so that $r_l(t)$ is constant and the boundary is stationary (waiting). If $\hat{r}(t)$ follows a CMF trajectory then, in the absence of accumulation/ablation, the velocity of the moving coordinate $\hat{r}(t)$ is given by

$$U = \frac{2}{n+2} A \, (\rho_{\mathrm{i}} g)^n \gamma(t)^n (r_l(t) - \hat{r}(t))^{(2n+1)\gamma(t) - n} g_l(t)^{2n+1} \tag{18}$$

Asymptotically, except at the boundary itself, this velocity is finite and positive, since $U > 0$ and its spatial derivative $\partial U/\partial r < 0$ sufficiently close to the boundary, showing that the distance $r_l(t) - \hat{r}(t)$ decreases with time.

In the absence of accumulation/ablation, therefore, conservation of mass fractions implies that $(r_l(t) - \hat{r}(t))U(t, \hat{r}(t))g_l(t)$ is constant in time. Thus, from (16), for points $\hat{r}(t)$ sufficiently

close to the boundary $(r_l(t) - \hat{r}(t))^{\gamma(t)+1} g_l(t)$ is constant in time. Hence, since $(r_l(t) - \hat{r}(t))$ is decreasing, $\gamma(t)$ is also decreasing. When $\gamma(t)$ reaches $n/(2n+1)$ the boundary moves.

It is a technical exercise to show that this property extends to cases with accumulation/ablation and with a general bedrock with a finite slope $\partial b/\partial r$ at the margin (see Partridge, 2013). The key point to notice is that the asymptotic behaviour depends on an infinite slope of h at the margin whereas $b(r)$ always has a finite slope.

3.5   Numerics

We now implement a numerical scheme using a finite difference method. The complete algorithm is detailed in Appendix B. In addition, we explain in Appendix B.6 why our implementation respects the asymptotic behaviour of the ice sheet at its margin.

4   Numerical results

This section is dedicated to the validation of the numerical scheme derived from the moving point method detailed in Sect. 3 and to the study of its behaviour. Every numerical experiment is performed with the parameter values given in Table 1.

4.1   Steady states with flat bedrock

We start by studying the behaviour of the numerical scheme using a surface mass balance $m(r)$ constant in time in order to define a steady state. When the steady state is reached, from Eq. (5), the following relationship is valid:

$$r\, m = \frac{\partial}{\partial r}(r\, h^\infty\, U_r^\infty) \tag{19}$$

with $h^\infty(r)$ the thickness of the steady ice sheet and $U^\infty(r)$ the ice velocity. By integrating the previous equation and by including boundary conditions (Eqs. 6 and 7), the position of the margin r_l^∞ can be obtained from

$$\int_0^{r_l^\infty} r m(r)\, \mathrm{d}r = \int_0^{r_l^\infty} \frac{\partial}{\partial r}(r\, h^\infty\, U_r^\infty)\, \mathrm{d}r = [r\, h^\infty\, U_r^\infty]_0^\infty = 0 \tag{20}$$

If the bedrock is flat, the profile of the steady ice sheet can be obtained from Eqs. (19) and (4) as

$$h(r)^\infty = \left(\left(\frac{2n+1}{n\, \rho_i\, g} \right)^n \frac{n+2}{2A} \right)^{\frac{1}{2(n+1)}} \left(\int_r^{r_l^\infty} \left(\frac{1}{r'} \int_0^{r'} m(s)\, s\, \mathrm{d}s \right)^{\frac{1}{n}} \mathrm{d}r' \right)^{\frac{n}{2(n+1)}} \tag{21}$$

Therefore, if the chosen surface mass balance is simple enough, we have an analytical formula for r_l^∞ from Eq. (20) and the profile of the steady state can be approximated with high accuracy by numerical integration from Eq. (21) using a composite trapezoidal rule for example. This approach was already in use in the EISMINT intercomparison project (Huybrechts et al., 1996) with the following constant-in-time surface mass balance

$$m(r) = \min\left(0.5\,\mathrm{m\,a^{-1}}, 10^{-2}\,\mathrm{m\,a^{-1}\,km^{-1}} \cdot (450\,\mathrm{km} - r) \right) \tag{22}$$

Finding r_l from Eq. (20) requires the solution of a cubic equation. A numerical approximation is $r_l \approx 579.81\,\mathrm{km}$.

As a first test, we consider initialising our numerical model with the following profile:

$$h(t_0, r) = h_0 \left(1 - \left(\frac{r}{r_l(t_0)} \right)^2 \right)^p \tag{23}$$

and study the convergence towards the steady state in three different cases. In each experiment, the initial grid has 21 points and the model is run for $10\,000\,\mathrm{a}$ with a constant time step $\Delta t = 0.1\,\mathrm{a}$. We now detail the initial state for each experiment:

a. Uniformly distributed initial grid with $r_l(0) = 450\,\mathrm{km}$, $h_0 = 1000\,\mathrm{m}$ and $p = 3/7$.

b. Initial grid with $r_l(0) = 500\,\mathrm{km}$ with higher resolution near the margin, $h_0 = 1000\,\mathrm{m}$ and $p = 1$.

c. Uniformly distributed initial grid with $r_l(0) = 600\,\mathrm{km}$, $h_0 = 4000\,\mathrm{m}$ and $p = 1/4$.

The evolution of the geometry and the overall motion of the grid points are shown for each experiment in Fig. 2. The three experiments show the convergence of every initial state towards the same steady state. These experiments also show the ability of the CMF method to capture the trajectory of the moving ice sheet margin (in advance and retreat).
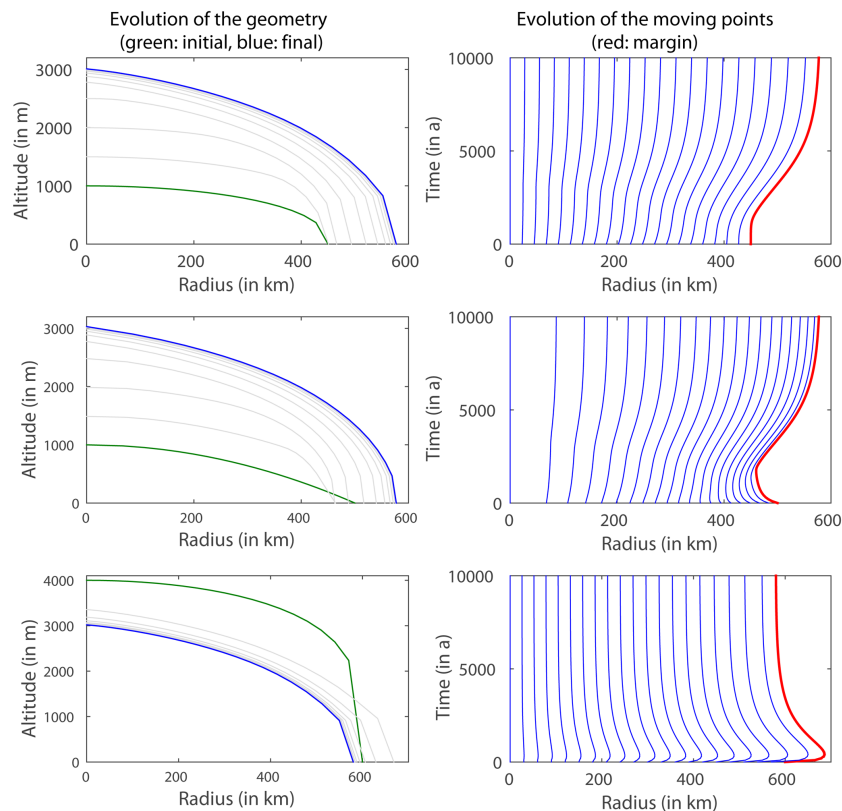

Figure 2: Evolution of the geometry and overall motion of the grid points for three experiments with the EISMINT surface mass balance and initial profile described by Eq. (23). Top: initial uniform grid with $r_l(0) = 450\,\mathrm{km}$, $h_0 = 1000\,\mathrm{m}$ and $p = 3/7$, middle: initial grid with higher resolution near the margin with $r_l(0) = 500\,\mathrm{km}$, $h_0 = 1000\,\mathrm{m}$ and $p = 1$, bottom: initial uniform grid with $r_l(0) = 600\,\mathrm{km}$, $h_0 = 4000\,\mathrm{m}$ and $p = 1/4$.
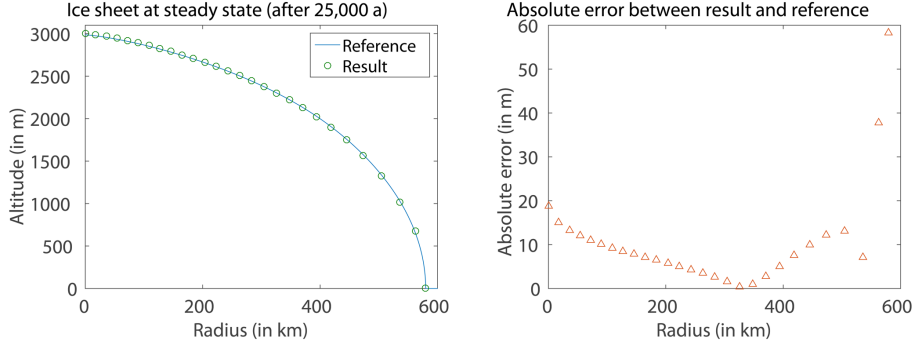
Figure 3: The steady state from the EISMINT moving-margin experiment compared with our 25 000 a model run with 28 nodes, uniformly distributed at the initial time. The reference profile is obtained by a numerical integration of Eq. (21) using a composite trapezoidal rule. The error in the ice thickness occurs mostly near the ice sheet margin, as in other experiments (RMS error is 15.71 m and maximum error is 58.23 m). The position of the margin is well determined as the absolute error is only 138.5 m.

We now perform the moving-margin EISMINT experiment (Huybrechts et al., 1996) in order to validate our numerical model in this case. At the initial time $t = 0$ we prescribe a uniformly distributed grid with $r_l(0) = 450$ km and an initial ice thickness $h(0, r)$ taken as $\Delta t \cdot m(r)$ for the constant time step $\Delta t = 0.1$ a. Then we run the model as in the EISMINT experiment for 25 000 a to reach the steady state. As we also want to compare our scheme with numerical models used in EISMINT, we first perform a model run with 28 nodes. With the same number of grid points as used in the fixed grid models included in EISMINT we are able to obtain a very good estimation for the position of the margin at steady state (commiting an absolute error of only 138.5 m for an exact position $r_l^\infty \approx 579.81$ km) without losing accuracy on the ice thickness (see Fig. 3). The estimation of the ice thickness at the ice divide is 3005.8 m compared to 2982.3 ± 26.4 m obtained by 2-D fixed grid models (we exclude 3-D models from our comparison as we only use radial symmetry, see Huybrechts et al., 1996) and compared to 2987 ± 0.01 m obtained by a numerical integration of Eq. (21) that we carried out by using a composite trapezoidal rule.

We also study the convergence of our method towards the reference solution in this case when the number of grid points is increased. We observe that the error for the margin position decreases at an almost quadratic rate $O(n_r^{1.95})$ and the error in the ice thickness at the ice divide at a linear rate $O(n_r^{1.16})$ (results obtained by performing experiments with an initial uniformly spaced grid with $n_r = 20, 28, 40, 60$ and 80 grid points).

4.2   Steady states with non-flat bedrock

The steady state approach of the previous section is still valid for an ice sheet lying on a non-flat bedrock. However, the experiments in such cases are quite limited as we only have the position of the steady margin from Eq. (20). Nevertheless we carry out a few experiments in this context in order to demonstrate that the CMF moving point approach is perfectly suitable for non-flat bedrock.

We consider the following fixed bedrock elevation:

$$b(r) = 2000\,\text{m} - 2000\,\text{m} \cdot \left(\frac{r}{300\,\text{km}}\right)^2 + 1000\,\text{m} \cdot \left(\frac{r}{300\,\text{km}}\right)^4$$
$$- 150\,\text{m} \cdot \left(\frac{r}{300\,\text{km}}\right)^6 \tag{24}$$

As in the previous section, experiments are performed with the EISMINT surface mass balance (Eq. 22). At an initial time $t = 0$ we prescribe a uniformly distributed grid with a margin located at $r_l(0) = 450\,\text{km}$ and an initial ice thickness $h(0, r) = \Delta t \cdot m(r)$ for the constant time step $\Delta t = 0.1\,\text{a}$. The resulting evolution of the geometry and the overall motion of the grid points are shown for a grid of 20 points in Fig. 4. We also study the convergence of our method towards the steady state when the number of grid points is increased. Again we observe that the error for the margin position decreases at a nearly quadratic rate $O(n_r^{1.83})$ (results obtained by performing experiments with an initial uniformly spaced grid and n_r grid points, $n_r = 20, 30, 40, 60$ and 80).
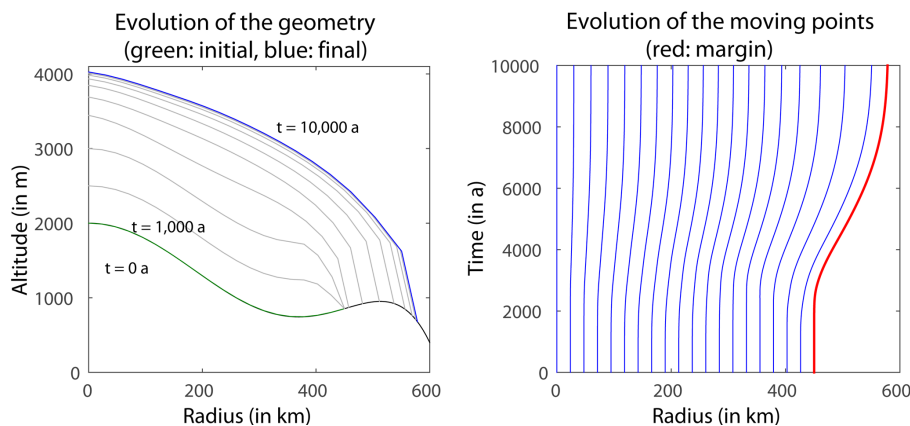

Figure 4: Evolution of the geometry and overall motion of the grid points for the non-flat bedrock (topography given in Eq. 24) with the EISMINT surface mass balance. At steady state, the observed error for the position of the margin is $127.7\,\text{m}$.

4.3 Validation with time-dependent solutions

In the previous paragraphs, steady states were used to validate our numerical CMF moving point numerical method. However these experiments did not validate the transient behaviour of the ice sheet margin. To do so, we use exact time-dependent solutions.

Few exact solutions for isothermal shallow ice sheets have been derived in the literature. Most are based on the similarity solutions established by Halfar (1981, 1983) for a zero surface mass balance. Bueler et al. (2005) extended this work to non-zero surface mass balance and established a new family of similarity solutions by adopting the following parameterised form for the surface mass balance,

$$m^{(\varepsilon)}(t, r) = \frac{\varepsilon}{t} h^{(\varepsilon)}(t, r) \tag{25}$$

with ε a real parameter in the interval $\left(\frac{-1}{2n+1}, +\infty\right)$. Assuming that $t > 0$ this leads to the
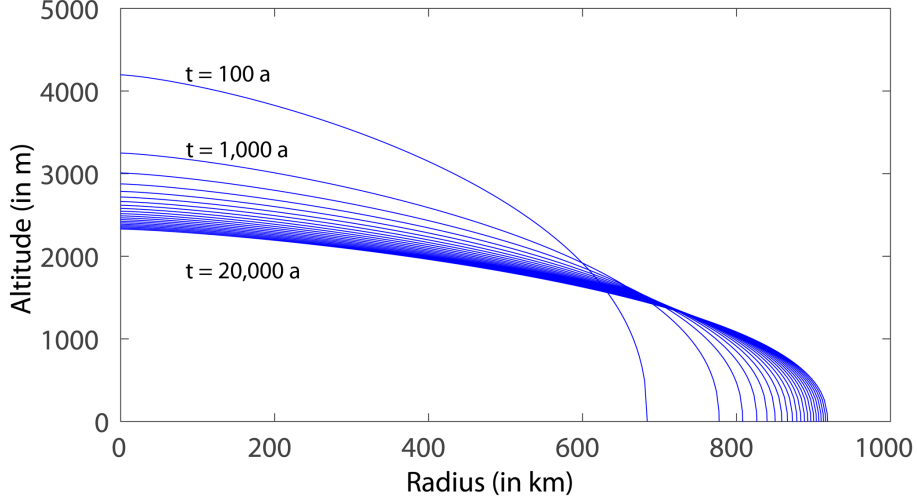
Figure 5: The reference ice sheet profile ($\varepsilon = 0$) displayed for $t = 100\,\mathrm{a}$, $t = 1000\,\mathrm{a}$, and at $1000\,\mathrm{a}$ intervals thereafter. Rapid changes occur in the state of the sheet at the beginning of the simulation, then the dynamics dramatically slow. The ice thickness at the ice divide decreases at a rate $t^{-1/9}$ and the position of the margin increases at a rate $t^{1/18}$.

following family of similarity solutions

$$h^{(\varepsilon)}(t, r) = \frac{1}{t^{\alpha(\varepsilon)}} \left(h_{0,1}^{\frac{2n+1}{n}} - \Lambda(\varepsilon) \left(\frac{r}{t^{\beta(\varepsilon)}} \right)^{\frac{n+1}{n}} \right)^{\frac{n}{2n+1}} \quad \text{for} \quad r \in \left[0, t^{\beta(\varepsilon)} \Theta(\varepsilon) \right] \tag{26}$$

with

$$\alpha(\varepsilon) = \frac{2 - (n+1)\varepsilon}{5n + 3}, \quad \beta(\varepsilon) = \frac{1 + (2n+1)\varepsilon}{5n + 3} \tag{27}$$

and

$$\Lambda(\varepsilon) = \frac{2n+1}{n+1} \left(\frac{(n+2)\beta(\varepsilon)}{2A(\rho_i\, g)^n} \right)^{\frac{1}{n}}, \quad \Theta(\varepsilon) = h_{0,1}^{\frac{2n+1}{n+1}} \Lambda(\varepsilon)^{-\frac{n}{n+1}} \tag{28}$$

The total mass of such ice sheets, as defined in Eq. (9), is

$$\theta^{(\varepsilon)}(t) = \beta(\varepsilon)^{-\frac{2}{n+1}} t^{\varepsilon} W_1 \tag{29}$$

where W_1 is a constant independent of ε

$$W_1 = 2\pi \int_0^{\Theta(1)} s \left(h_{0,1}^{\frac{2n+1}{n}} - \Lambda(1) s^{\frac{n+1}{n}} \right)^{\frac{n}{2n+1}} \mathrm{d}s \tag{30}$$

We study in this section the accuracy of transient model runs in comparison with the time-dependent exact solutions. The initialisation of every experiment is done by using the exact time-dependent solution (Eq. 26) and, at each time step, the surface mass balance is evaluated at each moving node by using the relationship $m = \frac{\varepsilon}{t} h$ from Eq. (25). When ε is non-zero, some *feedback* between the surface mass balance and the ice thickness is expected (Leysinger Vieli and Gudmundsson, 2004). Each model run in this section uses a fixed time step of $\Delta t = 0.01\,\mathrm{a}$.

The first experiment is conducted with the constant mass similarity solution ($\varepsilon = 0$) between $t = 100\,\mathrm{a}$ and $t = 20\,000\,\mathrm{a}$ for the reference period (Fig. 5). We first analyse the results obtained

with a grid made up of 100 nodes, uniformly distributed at the initial time. In terms of thickness, errors mostly occur near the ice sheet margin (Fig. 6) as is the case with fixed grid methods (see Bueler et al., 2005). However, the position of the ice sheet margin is well estimated, the estimated error being kept under one kilometer (Fig. 7).
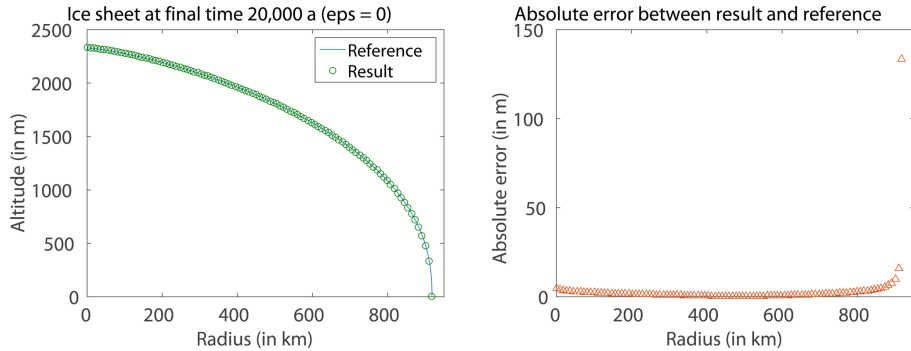

Figure 6: The result obtained at final time $t = 20\,000\mathrm{a}$ for $\varepsilon = 0$ with 100 nodes equally distributed at initial time $t = 100\,\mathrm{a}$ and a fixed time step $\Delta t = 0.01\,\mathrm{a}$ is compared to the reference. A maximum error of $134\,\mathrm{m}$ on the ice thickness is obtained at the margin, while the interior of the sheet has errors less than $10\,\mathrm{m}$. The position of the margin is obtained with an error of $880\,\mathrm{m}$.
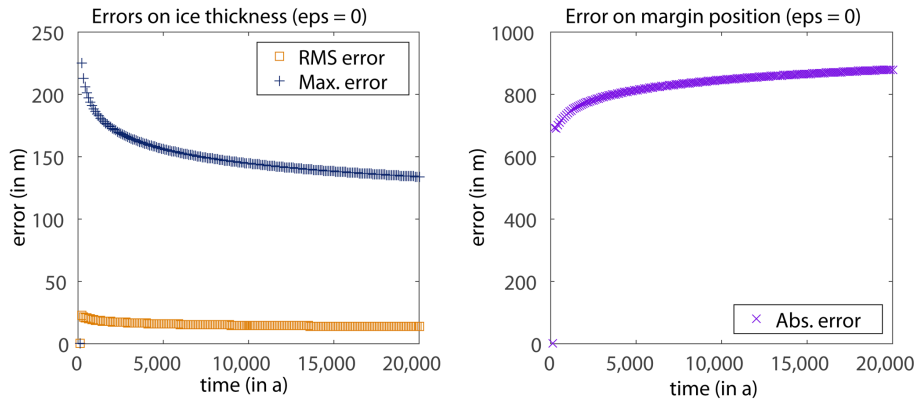

Figure 7: Evolution of the RMS error and maximum absolute error in the ice thickness, and absolute error in the position of the margin during the run, for the case $\varepsilon = 0$ with 100 nodes equally distributed at initial time $t = 100\,\mathrm{a}$ and a fixed time step $\Delta t = 0.01\,\mathrm{a}$. Errors in the ice thickness decrease as the ice sheet slows down. The errors in the position of the margin increase in time but their evolution is slower when the dynamics are slower.

We then study the convergence of our scheme at a final time $t = 20\,000\,\mathrm{a}$ when the number of grid points is increased. We perform the same analysis for $\varepsilon = -1/8, 1/4$ and $3/4$. Rates of convergence for different errors are summarised in Table 2.

5   Conclusions

In this paper, we introduced a moving point approach for ice sheet modelling using the SIA (including non-flat bedrock) based on the conservation of local mass. From this principle we

Table 2: Rate of convergence of different errors between numerical results obtained for time-dependent solutions at time $t = 20\,000\,\text{a}$. The different estimated rates of convergence are obtained by performing experiments with $n_r = 10, 20, 40, 60, 80, 100$ and 200 grid points for different configurations of surface mass balance (Eq. 25).

	$\varepsilon = 0$	$\varepsilon = -1/8$	$\varepsilon = 1/4$	$\varepsilon = 3/4$
RMS error on h	$O(n_r^{-1.07})$	$O(n_r^{-1.10})$	$O(n_r^{-1.10})$	$O(n_r^{-1.12})$
Max. error on h	$O(n_r^{-0.57})$	$O(n_r^{-0.60})$	$O(n_r^{-0.59})$	$O(n_r^{-0.60})$
error on r_l	$O(n_r^{-1.32})$	$O(n_r^{-1.41})$	$O(n_r^{-1.38})$	$O(n_r^{-1.41})$
error on total volume	-	$O(n_r^{-1.24})$	$O(n_r^{-1.43})$	$O(n_r^{-1.43})$

derived an efficient finite-difference moving point scheme allowing rapid computation of the solutions. The scheme was validated by comparing results with steady states from the EISMINT benchmark (Huybrechts et al., 1996) and time-dependent solutions from Bueler et al. (2005). Accurate results have been obtained with a small number of grid points in both cases. Hence the comparison shows that the approach has considerable potential for future investigations.

Whilst this paper uses a vertically averaged horizontal ice velocity given by the shallow ice approximation, the moving mesh scheme is independent of the *form* of the ice velocity used here and could be used as a solver for mass balance alongside more complex vertically-integrated approximations (see e.g. Schoof and Hindmarsh, 2010).

As mentioned earlier, the conservation approach is suitable not only for 1-D-cases (flowline or radial) but also for 2-D-scenarios. A first application has been demonstrated in Partridge (2013) and will be the subject of a new paper. The conservation approach can also be applied to marine ice sheets. In these cases, different kinds of boundaries have to be considered: e.g. grounding line, shelf front, and continental margin. However, the problem of initialisating such a model for use in real applications remains open. The incorporation of various data assimilation procedures is currently being investigated in this context.

A Consistency of the moving point approach at boundaries

We now verify that $\mathrm{d}\hat{r}/\mathrm{d}t$ tends to the velocity obtained from Eq. (8) at the ice margin when $\hat{r}(t)$ tends to $r_l(t)$. Assuming the continuity of $\partial h/\partial r$ and m in the vicinity of the ice sheet margin, by L'Hôpital's rule

$$\lim_{\hat{r}(t)\to r_l(t)} \frac{\mathrm{d}\hat{r}}{\mathrm{d}t} = U(t, r_l) + \lim_{\hat{r}(t)\to r_l(t)} \left(\frac{\frac{\dot{\theta}}{\theta}\hat{r}h(t,\hat{r}) - \hat{r}m(t,\hat{r})}{h(t,\hat{r}) + \hat{r}\frac{\partial h}{\partial r}(t,\hat{r})} \right) \tag{31}$$

This gives

$$\lim_{\hat{r}(t)\to r_l(t)} \frac{\mathrm{d}\hat{r}}{\mathrm{d}t} = U(t, r_l) - m(t, r_l)\left(\frac{\partial h}{\partial r}(t, r_l) \right)^{-1} \tag{32}$$

The limit is consistent with the velocity of the moving margin obtained in Eq. (8). The same approach can be used to show that $\mathrm{d}\hat{r}/\mathrm{d}t$ tends to 0 when $\hat{r}(t)$ tends to the ice divide $r = 0$.

B   A finite difference algorithm

The moving point method is discretised on a radial line using finite differences on the grid $\{\hat{r}_i\}$, $i = 1, \ldots, n_r$ where

$$0 = \hat{r}_1(t) < \hat{r}_2(t) < \ldots < \hat{r}_{n_r-1}(t) < \hat{r}_{n_r}(t) = r_l(t), \tag{33}$$

The approximation of $h(t, r)$ at $\hat{r}_i(t_k) = \hat{r}_i^k$ is written h_i^k and that of the ice velocity $U(t, r)$ as U_i^k. The velocity of the points is represented by v_i^k. The symbol θ^k designates the numerical approximation of the total mass and the constant mass fractions are represented by μ_i for every $\mu(\hat{r}_i^k)$.

Before giving the formula for every quantity calculated, we give the structure of the finite difference algorithm in Algorithm 1.

Algorithm 1 Finite difference moving point algorithm

Require: $\{\hat{r}_i^0\}$ and $\{h_i^0\}$, $i = 1, \ldots, n_r$ with $\hat{r}_1^0 = 0$ and $h_{n_r}^0 = 0$.
 1: Compute total mass θ^0 with eq. (34)
 2: Compute mass fractions μ_i, $i = 1, \ldots, n_r$, with eq. (35)
 3: **while** $t < t_{end}$ **do**
 4:     Compute ice velocities U_i^k with eq. (36) and eq. (37)
 5:     Compute point velocities v_i^k with eq. (38) and eq. (39)
 6:     Update total mass θ^{k+1} with eq. (40)
 7:     Update moving point positions $\hat{r}_i^{k+1}$ with eq. (41)
 8:     Update ice thickness h_i^{k+1} with eq. (42) and (43)
 9:     $k \leftarrow k + 1$
10:     $t \leftarrow t + \Delta t$
11: **end while**

B.1   Initialisation

At the initial time the user needs to provide the initial location of each grid point $\{\hat{r}_i^0\}$ and the initial ice thickness $\{h_i^0\}$ there. By definition, we assume that $\hat{r}_1^0 = 0$ and $h_{n_r}^0 = 0$. We estimate the total mass of the ice sheet at the initial time by using a composite trapezoidal rule approximating Eq. (9). This gives:

$$\theta^0 = \frac{\pi}{2} \sum_{j=1}^{n_r-1} \left(h_j^0 + h_{j+1}^0 \right) \left(\left(\hat{r}_{j+1}^0 \right)^2 - \left(\hat{r}_j^0 \right)^2 \right) \tag{34}$$

We derive the numerical approximation for the mass fractions μ_i by discretising Eq. (11) following the same principle:

$$\mu_1 = 0, \qquad \mu_i = \frac{\pi}{2\,\theta^0} \sum_{j=1}^{i-1} \left(h_j^0 + h_{j+1}^0 \right) \left(\left(\hat{r}_{j+1}^0 \right)^2 - \left(\hat{r}_j^0 \right)^2 \right) \tag{35}$$

B.2 Ice velocities

We confine the algorithm to $n = 3$ for the exponent in the Glen flow law. Then Eq. (4) giving the ice velocity can be expanded by using the binomial theorem:

$$
\begin{aligned}
|U(t,r)| = \frac{2}{5} A \, (\rho_{\mathrm{i}} g)^3 \bigg| \, h^4 \left(\frac{\partial b}{\partial r} \right)^3 + \frac{3}{5} \frac{\partial (h^5)}{\partial r} \left(\frac{\partial b}{\partial r} \right)^2 \\
+ \frac{1}{3} \left(\frac{\partial (h^3)}{\partial r} \right)^2 \frac{\partial b}{\partial r} + \frac{27}{343} \left(\frac{\partial (h^{7/3})}{\partial r} \right)^3 \bigg|
\end{aligned}
\tag{36}
$$

We choose to rewrite the radial form of Eq. (4) in this way in order to ensure that the ice velocity at the ice sheet margin computed with a finite difference scheme can be non-zero as noted in Sect. 3.4. The bedrock elevation b and its derivative are known for every location of the domain. The sign of U_i^k ($U_1^k = 0$) is obtained by calculating the sign of $s_i^k - s_{i-1}^k$ (approximating the sign of the surface slope by an upwind scheme). We also approximate the derivatives of h^p for any $p > 0$ by an upwind scheme:

$$
\left. \frac{\partial (h^p)}{\partial r} \right|_{r = r_i^k} = \frac{\left(h_i^k \right)^p - \left(h_{i-1}^k \right)^p}{r_i^k - r_{i-1}^k}
\tag{37}
$$

B.3 Approximate nodal velocities

The velocity of interior nodes is obtained by discretising Eq. (14) as

$$
v_1^k = 0, \qquad v_i^k = U_i^k + \frac{1}{2 \, \hat{r}_i^k \, h_i^k} \left(\mu_i \int_0^{\hat{r}_{n_r}^k} m(t^k, r) \, \mathrm{d} \left(r^2 \right) - \int_0^{\hat{r}_i^k} m(t^k, r) \, \mathrm{d} \left(r^2 \right) \right)
\tag{38}
$$

where the integrals in Eq. (38) are approximated by a composite trapezoidal rule. For the velocity of the ice sheet margin, Eq. (8) is discretised by using an order-1 upwind scheme, namely,

$$
v_{n_r}^k = U_{n_r}^k - m \left(t^k, r_{n_r}^k \right) \frac{\hat{r}_{n_r}^k - \hat{r}_{n_r-1}^k}{h_{n_r}^k - h_{n_r-1}^k}
\tag{39}
$$

B.4 Time stepping

The total mass θ^{k+1} is updated by using an explicit Euler scheme

$$
\theta^{k+1} = \theta^k + \Delta t \, \dot{\theta}^k = \theta^k + \Delta t \, \pi \int_0^{\hat{r}_{n_r}^k} m(t,r) \mathrm{d} \left(r^2 \right)
\tag{40}
$$

Again the integral is approximated by a composite trapezoididal rule.

As in the case of the total mass, the position of the nodes is updated by using an explicit Euler scheme

$$
\hat{r}_i^{k+1} = \hat{r}_i^k + \Delta t \, v_i^k
\tag{41}
$$

with Δt small enough to preserve the order in Eq. (33).

B.5 Approximate ice thickness

The ice thickness for interior nodes h_i^{k+1} is recovered algebraically at the new time using an order-2 midpoint approximation of Eq. (15), namely,

$$h_i^{k+1} = \frac{\theta^{k+1}}{\pi} \frac{\mu_{i+1} - \mu_{i-1}}{\left(\hat{r}_{i+1}^{k+1}\right)^2 - \left(\hat{r}_{i-1}^{k+1}\right)^2} \tag{42}$$

The ice thickness at the ice divide h_1^{k+1} is obtained by using the order-1 upwind scheme.

$$h_1^{k+1} = \frac{\theta^{k+1}}{\pi} \frac{\mu_2 - \mu_1}{\left(\hat{r}_2^{k+1}\right)^2 - \left(\hat{r}_1^{k+1}\right)^2} \tag{43}$$

B.6 Behaviour of the approximate ice velocity at the ice margin

As in Sect. 3.4, assuming the topography of the bedrock is flat at the vicinity of the margin, the asymptotic form of the radial ice velocity is

$$U = \frac{2}{n+2} A \, (\rho_{\mathrm{i}}g)^n \gamma^n (r_l - r)^{(2n+1)\gamma - n} g_l^{2n+1} \tag{44}$$

Hence the leading term in the numerical approximation (Eq. 36) to the ice velocity at the approximation h_l to the ice margin is

$$
\begin{aligned}
&- \frac{2}{5} \operatorname{sgn} (s_{n_r} - s_{n_r-1}) A \, (\rho_{\mathrm{i}}g)^3 \left(\frac{3}{7}\right)^3 \left| \frac{h_{n_r}^{7/3} - h_{n_r-1}^{7/3}}{\hat{r}_{n_r} - \hat{r}_{n_r-1}} \right|^3 \\
&= -\frac{2}{5} \operatorname{sgn} (s_{n_r} - s_{n_r-1}) A \, (\rho_{\mathrm{i}}g)^3 \left(\frac{3}{7}\right)^3 \left| \frac{h_{n_r-1}^{7/3}}{\hat{r}_{n_r} - \hat{r}_{n_r-1}} \right|^3
\end{aligned}
\tag{45}
$$

since $h_{n_r} = 0$. But from Eq. (44) the asymptotic analytic ice velocity (when $n = 3$) is

$$\frac{2}{5} A \, (\rho_{\mathrm{i}}g)^3 \left(\frac{3}{7}\right)^3 (r_{n_r} - r)^{7\gamma-3} g_I^7 = \frac{2}{5} A \, (\rho_{\mathrm{i}}g)^3 \frac{27}{343} \left(\frac{h(r)^{7/3}}{r_{n_r} - r}\right)^3 \tag{46}$$

by Eq. (16). Hence the numerical approximation to the ice velocity has the same asymptotic behaviour as the asymptotic analytic ice velocity with $n = 3$. The result also holds for general n.

References

M. J. Baines, M. E. Hubbard, and P. K. Jimack. A moving mesh finite element algorithm for the adaptive solution of time-dependent partial differential equations with moving boundaries. *Appl. Numer. Math.*, 54(3):450–469, 2005. doi: 10.1016/j.apnum.2004.09.013.

M. J. Baines, M. E. Hubbard, and P. K. Jimack. Velocity-based moving mesh methods for nonlinear partial differential equations. *Commun. Comput. Phys.*, 10(3):509–576, 2011. doi: 10.4208/cicp.201010.040511a.

K. W. Blake. *Moving mesh methods for Non-Linear Parabolic Partial Differential Equations*. PhD thesis, University of Reading, Reading, Berks., UK, Oct. 2001. URL `http://www.reading.ac.uk/web/FILES/maths/Kw_blake.pdf`.

C. J. Budd, W. Huang, and R. D. Russell. Adaptivity with moving grids. *Acta Numerica*, 18: 111–241, 2009. doi: 10.1017/S0962492906400015.

E. Bueler, C. S. Lingle, J. A. Kallen-Brown, D. N. Covey, and L. N. Bowman. Exact solutions and verification of numerical models for isothermal ice sheets. *J. Glaciol.*, 51(173):291–306, 2005. doi: 10.3189/172756505781829449.

N. Calvo, J. I. Díaz, J. Durany, E. Schiavi, and C. Vázquez. On a doubly nonlinear parabolic obstacle problem modelling ice sheet dynamics. *SIAM J. Appl. Math.*, 63(2):683–707, 2002. doi: 10.1137/S0036139901385345.

W. Cao, W. Huang, and R. D. Russell. Approaches for generating moving adaptive meshes: location versus velocity. *Appl. Numer. Math.*, 47(2):121–138, 2003. doi: 10.1016/S0168-9274(03) 00061-8.

J. A. Church, P. U. Clark, A. Cazenave, J. M. Gregory, S. Jevrejeva, A. Leverman, M. A. Merrifield, G. A. Milne, R. S. Nerem, P. D. Nunn, A. J. Payne, W. T. Pfeffer, D. Stammer, and A. S. Unnikrishnan. Sea level change. In T. F. Stocker, D. Qin, G.-K. Plattner, M. Tignor, S. K. Allen, J. Boschung, A. Nauels, Y. Xia, V. Bex, and P. M. Midgley, editors, *Climate Change 2013: The Physical Science Basis. Contribution of Working Group I to the Fifth Assessment Report of the Intergovernmental Panel on Climate Change*, pages 1137–1216. Cambridge University Press, Cambridge, United Kingdom and New York, NY, USA, 2013.

S. L. Cornford, D. F. Martin, D. T. Graves, D. F. Ranken, A. M. Le Brocq, R. M. Gladstone, A. J. Payne, E. G. Ng, and W. H. Lipscomb. Adaptive mesh, finite volume modeling of marine ice sheets. *J. Comput. Phys.*, 232:529–549, 2013. doi: 10.1016/j.jcp.2012.08.037.

K. M. Cuffey and W. S. B. Paterson. *The physics of glaciers (fourth edition)*. Butterworth-Heinemann/Elsevier, Burlington, MA, USA and Oxford, UK, 2010.

A. C. Fowler. Modelling ice sheet dynamics. *Geophys. Astro. Fluid*, 63(1-4):29–65, 1992. doi: 10.1080/03091929208228277.

O. Gagliardini, T. Zwinger, F. Gillet-Chaulet, G. Durand, L. Favier, B. de Fleurian, R. Greve, M. Malinen, C. Martín, P. Råback, J. Ruokolainen, M. Sacchettini, M. Schäfer, H. Seddik, and J. Thies. Capabilities and performance of Elmer/Ice, a new-generation ice sheet model. *Geosci. Model Dev.*, 6(4):1299–1318, 2013. doi: 10.5194/gmd-6-1299-2013.

J. W. Glen. The creep of polycrystalline ice. *P. Roy. Soc. A.-Math. Phy.*, 228(1175):519–538, 1955.

P. Halfar. On the dynamics of the ice sheets. *J. Geophys. Res.-Oceans*, 86(C11):11065–11072, 1981. doi: 10.1029/JC086iC11p11065.

P. Halfar. On the dynamics of the ice sheets 2. *J. Geophys. Res.-Oceans*, 88(C10):6043–6051, 1983. doi: 10.1029/JC088iC10p06043.

R. C. A. Hindmarsh. Qualitative dynamics of marine ice sheets. In *Ice in the climate system*, pages 67–99. Springer, Berlin, Heidelberg, Germany, 1993.

R. C. A. Hindmarsh and E. Le Meur. Dynamical processes involved in the retreat of marine ice sheets. *J. Glaciol.*, 47(157):271–282, 2001. doi: 10.3189/172756501781832269.

K. Hutter. *Theoretical Glaciology*. D. Reidel, Dordrecht, the Netherlands, 1983.

P. Huybrechts, A. J. Payne, and The EISMINT Intercomparison Group. The EISMINT benchmarks for testing ice-sheet models. *Ann. Glaciol.*, 23:1–12, 1996.

T. E. Lee, M. J. Baines, and S. Langdon. A finite difference moving mesh method based on conservation for moving boundary problems. *J. Comput. Appl. Math.*, 288:1–17, 2015. doi: 10.1016/j.cam.2015.03.032.

G. J. Leysinger Vieli and G. H. Gudmundsson. On estimating length fluctuations of glaciers caused by changes in climatic forcing. *J. Geophys. Res.-Earth*, 109(F01007), 2004. doi: 10.1029/2003JF000027.

D. Partridge. *Numerical modelling of glaciers: moving meshes and data assimilation*. PhD thesis, University of Reading, Reading, Berks, UK, June 2013. URL `http://www.reading.ac.uk/web/FILES/maths/DP_PhDThesis.pdf`.

F. Pattyn, L. Périchon, G. Durand, L. Favier, O. Gagliardini, R. C. A. Hindmarsh, T. Zwinger, T. Albrecht, S. Cornford, D. Docquier, J. J. Fürst, D. Goldberg, G. H. Gudmundsson, A. Humbert, M. Hütten, P. Huybrechts, G. Jouvet, T. Kleiner, E. Larour, D. Martin, M. Morlighem, A. J. Payne, D. Pollard, M. Rückamp, O. Rybak, H. Seroussi, M. Thoma, and N. Wilkens. Grounding-line migration in plan-view marine ice-sheet models: results of the ice2sea MISMIP3d intercomparison. *J. Glaciol.*, 59(215):410–422, 2013. doi: 10.3189/2013JoG12J129.

A. J. Payne, P. Huybrechts, A. Abe-Ouchi, R. Calov, J. L. Fastook, R. Greve, S. J. Marshall, I. Marsiat, C. Ritz, L. Tarasov, and M. P. A. Thomassen. Results from the EISMINT model intercomparison: the effects of thermomechanical coupling. *J. Glaciol.*, 46(153):227–238, 2000. doi: 10.3189/172756500781832891.

G. Scherer and M. J. Baines. Moving mesh finite difference schemes for the porous medium equation. Mathematics Report Series 1/2012, Department of Mathematics and Statistics, University of Reading, Reading, Berks, UK, 2012. URL `https://www.reading.ac.uk/web/FILES/maths/godelareport.pdf`.

C. Schoof and R. C. A. Hindmarsh. Thin-film flows with wall slip: an asymptotic analysis of higher order glacier flow models. *Q. J. Mech. Appl. Math.*, 63(1):73–114, 2010. doi: 10.1093/qjmam/hbp025.

G. G. Stokes. On the Theories of Internal Friction of Fluids in Motion. *Transactions of the Cambridge Philosophical Society*, 8:287–305, 1845.

A. Vieli and A. J. Payne. Assessing the ability of numerical ice sheet models to simulate grounding line migration. *J. Geophys. Res.-Earth*, 110(F01003), 2005. doi: 10.1029/2004JF000202.